Multiple-point and multiple-time correlation functions in a hard-sphere fluid

Ramses van Zon and Jeremy Schofield

Chemical Physics Theory Group, Department of Chemistry, University of Toronto, Toronto, Ontario, Canada M5S 3H6

(Received 1 August 2001; published 18 December 2001)

A recent mode-coupling theory of higher-order correlation functions is tested on a simple hard-sphere fluid system at intermediate densities. Multiple-point and multiple-time correlation functions of the densities of conserved variables are calculated in the hydrodynamic limit and compared to results obtained from event-based molecular dynamics simulations. It is demonstrated that the mode-coupling theory results are in excellent agreement with the simulation results provided that dissipative couplings are included in the vertices appearing in the theory. In contrast, simplified mode-coupling theories in which the densities obey Gaussian statistics neglect important contributions to both the multiple point and multiple-time correlation functions on all time scales.

I. INTRODUCTION

Over the last few years, the emergence of multidimensional nuclear magnetic resonance (NMR) [1,2] and nonresonant nonlinear Raman [3–5] techniques has generated renewed interest in the information content of higher-order correlation functions involving time correlations of dynamical quantities at multiple points and time separations. These experimental developments hold great promise for the elucidation of the nature of the underlying dynamics giving rise to complex relaxation behavior in supercooled liquids, polymeric systems, and proteins [6–8]. Concurrently, simulation studies probing the microscopic origin of dynamical heterogeneity in dense systems [9] have made use of the increased information content available in multiple-point [10] and multiple-time [11] correlation functions.

Although there has been some recent work attempting to reproduce simulation results for the off-resonant fifth-order Raman response function [12–14], there has been little theoretical work to establish a microscopic theory for general higher-order correlation functions. In a previous article [15], a general mode-coupling theory was developed in which the long-time behavior for multiple-point and multiple-time correlation functions was expressed in terms of ordinary two-time, two-point correlation functions of a set of slow variables, which are coupled by vertices containing both static (called Euler) and dynamic (called dissipative) correlations. The theory is based upon the assumption that the long-time dynamics of arbitrary variables is a functional of a set of slow modes of the system. The long-time dynamics of higher-order correlation functions is then described by isolating the component of the relevant variables along multilinear products of the slow variables, resulting in expressions for the higher-order correlation functions in terms of the sum of an infinite number of multiple-point correlation functions of slow modes. The formulation is made tractable by a cumulant expansion method (called N ordering [16,17]) in which multiple-point correlation functions are factored into convolutions over the familiar two-point, two-time correlation functions of the slow modes. In this way, the need to simplify the mode-coupling expressions for higher-order correlation functions based on an assumption of Gaussian statis-

tical behavior of the slow modes is avoided. It was suggested that simple mode-coupling theories [18,19] based upon this Gaussian assumption lead to a relatively poor description of the long-time behavior of higher-order correlation functions.

The purpose of this article is to validate the mode-coupling theory expressions for multiple-point and multiple-time correlation functions by examining the simplest non-trivial system, the hard-sphere liquid. The hard-sphere liquid is a very useful system to examine theoretically since the simple form of the interaction potential allows static correlation functions to be related to the radial distribution function at contact. In turn, the radial distribution function can be approximated using an accurate equation of state, such as that of Carnahan and Starling [20], which relates the pressure to the density and the temperature. In addition, excellent predictions exist for dynamical properties of hard-sphere systems based on detailed kinetic theory [21]. Another advantage of looking at hard-sphere systems is that the dynamics of the system can be simulated very efficiently using event-based molecular dynamics methods [22] since particles evolve freely between collisions, thereby allowing good statistics to be obtained from simulations.

We shall focus on systems of moderate reduced densities ($\rho^* = 0.25$) in which "mode-coupling" effects leading to nonexponential relaxation of correlation functions of linear densities, such as the dynamical structure factor, can be neglected. In particular, we target correlation functions of long-wavelength fluctuations, which decay on long time scales and exhibit complicated higher-order correlation functions.

This paper is organized as follows. In Sec. II, the mode-coupling formalism developed in Ref. [15] is reviewed and adapted to the hard-sphere system. Explicit expressions are presented for three-point and three-time correlation functions involving linear densities of number (or mass), transverse, and longitudinal velocities. In Sec. III, simulation methods particularly suited for calculating higher-order correlation functions in a hard-sphere system are discussed. In Sec. IV, the predictions of the mode-coupling theory are compared to the simulation results for relatively simple three-point and three-time correlation functions, and it is demonstrated that dissipative parts of vertices provide additional important couplings to those at Euler order. The results are contrasted

with those obtained within the framework of the Gaussian mode-coupling theory [18,19]. Finally, conclusions of the study are given in Sec. V.

II. THEORETICAL FORMULATION

The system under consideration is composed of N particles of mass m and diameter a in a volume $V = L_x \times L_y \times L_z$. The particles interact through the two-body hard-sphere potential

$$V(r) = \begin{cases} 0 & \text{if } r < a, \\ \infty & \text{if } r \geq a. \end{cases} \qquad (1)$$

Given the form of the potential, the dynamics generated by the Hamiltonian conserves the total number of particles N, the total angular momentum, the linear momenta $\mathbf{P}$, and the energy E of the system. In Ref. [15], expressions for the long-time behavior of correlation functions were obtained under the assumption that the slowly varying part of an arbitrary dynamical variable is an analytic function of a set of slow variables $\mathbf{A}$ of the system. An essential part of successfully applying the formalism to a particular system is the identification of a *complete* set of slow variables. To identify the slow modes of the system, it is helpful to consider the local densities of the conserved variables N, $\mathbf{P}$, and E,

$$N(\mathbf{r}) = \sum_{i=1}^{N} \delta(\mathbf{r} - \mathbf{r}_i),$$

$$\mathbf{P}(\mathbf{r}) = \sum_{i=1}^{N} \mathbf{p}_i \delta(\mathbf{r} - \mathbf{r}_i),$$

$$E(\mathbf{r}) = \sum_{i=1}^{N} \left(\frac{p_i^2}{2m} + \frac{1}{2} \sum_{j \neq i} V(|\mathbf{r}_i - \mathbf{r}_j|) \right) \delta(\mathbf{r} - \mathbf{r}_i),$$

where $\mathbf{r}_i$ and $\mathbf{p}_i$ are the spatial position and momentum of particle i. Noting that the Fourier transforms of these densities,

$$N_{\mathbf{k}} = \sum_{i=1}^{N} e^{i\mathbf{k} \cdot \mathbf{r}_i},$$

$$\mathbf{P}_{\mathbf{k}} = \sum_{i=1}^{N} \mathbf{p}_i e^{i\mathbf{k} \cdot \mathbf{r}_i},$$

$$E_{\mathbf{k}} = \sum_{i=1}^{N} \left(\frac{p_i^2}{2m} + \frac{1}{2} \sum_{j \neq i} V(|\mathbf{r}_i - \mathbf{r}_j|) \right) c^{i\mathbf{k} \cdot \mathbf{r}_i}, \qquad (2)$$

are slowly varying quantities for small $k = |\mathbf{k}|$ since their time derivatives are proportional to k, the minimal set of slow variables $A'_{\mathbf{k}}$ must include all the "hydrodynamic" variables $\{N_{\mathbf{k}}, \mathbf{P}_{\mathbf{k}}, E_{\mathbf{k}}\}$ with k smaller than some cutoff wave vector k_c. For our purposes, it is convenient to work with a slightly different basis set $A_{\mathbf{k}}$, composed of the variables $N_{\mathbf{k}}$, $L_{\mathbf{k}} = \mathbf{P}_{\mathbf{k}}^x$, $T_{1\mathbf{k}} = \mathbf{P}_{\mathbf{k}}^y$, $T_{2\mathbf{k}} = \mathbf{P}_{\mathbf{k}}^z$, and $H_{\mathbf{k}} = (3N_{\mathbf{k}} - 2\beta E_{\mathbf{k}})/\sqrt{6}$, where $\beta = 1/(k_B T)$ is the inverse temperature

of the system, $\mathbf{P}_{\mathbf{k}}^z$ is the x component of the vector $\mathbf{P}_{\mathbf{k}}$, and $\mathbf{k}$ is taken along the x axis. Note that the $T_{1\mathbf{k}}$ and $T_{2\mathbf{k}}$ are the transverse modes of the momentum density, while $L_{\mathbf{k}}$ is the longitudinal momentum density. With this definition of the basis set, the matrix

$$\langle A_{\mathbf{k}}^a A_{\mathbf{k}}^{b*} \rangle = \langle A_{\mathbf{k}}^a A_{-\mathbf{k}}^b \rangle \delta_{a,b}$$

is diagonal in the hydrodynamic labels a and b, where $\langle \cdots \rangle$ denotes the grand-canonical ensemble average. The nonlinear dependence of the dynamical variables is expressed in terms of a "multilinear" basis set,

$$Q_0 \equiv 1,$$

$$Q_1 \equiv A_{\mathbf{k}} - \langle A_{\mathbf{k}} \rangle \equiv \hat{A}_{\mathbf{k}},$$

$$Q_2 \equiv Q_{\mathbf{k}-\mathbf{q}} Q_{\mathbf{q}} - \langle Q_{\mathbf{k}-\mathbf{q}} Q_{\mathbf{q}} \rangle - \langle Q_{\mathbf{k}-\mathbf{q}} Q_{\mathbf{q}} Q_1^* \rangle \cdot K_{11}^{-1} \cdot Q_1, \quad (3)$$

$$\vdots$$

where the "$\cdot$" notation denotes a sum over components of the column vector $A_{\mathbf{k}}$ (the indices of the hydrodynamic variables $N_{\mathbf{k}}$, $L_{\mathbf{k}}$, $T_{1\mathbf{k}}$, $T_{2\mathbf{k}}$, and $H_{\mathbf{k}}$). The subtractions in the basis set defined in Eq. (3) are included to ensure that the multilinear matrix,

$$K_{lm} = \langle Q_l Q_m^* \rangle = \langle Q_l Q_m^* \rangle \delta_{l,m}, \qquad (4)$$

is diagonal in *mode order* l. The slow part of any dynamical variable C is removed by the projection operator

$$\mathcal{P}C \equiv \sum_{l=0}^{\infty} \langle C Q_l^* \rangle K_{ll}^{-1} Q_l, \qquad (5)$$

and the complementary projection operator $\mathcal{P}_{\perp} = 1 - \mathcal{P}$ projects onto the orthogonal subspace.

Writing the three-point correlation function $\langle \hat{A}_{\mathbf{k}-\mathbf{q}}(t) \hat{A}_{\mathbf{q}}(t) \hat{A}_{-\mathbf{k}} \rangle$ in terms of the basis set, we obtain

$$\langle \hat{A}_{\mathbf{k}-\mathbf{q}}(t) \hat{A}_{\mathbf{q}}(t) \hat{A}_{-\mathbf{k}} \rangle = \langle \hat{A}_{\mathbf{k}}(t) \hat{A}_{-\mathbf{k}} \rangle \cdot K_{11}^{-1} \cdot \langle \hat{A}_{-\mathbf{k}} \hat{A}_{\mathbf{k}-\mathbf{q}} \hat{A}_{\mathbf{q}} \rangle$$
$$+ G_{\mathbf{k}-\mathbf{q},\mathbf{q};\mathbf{k}}^{21}(t) \cdot K_{11}, \qquad (6)$$

where $G^{mn}(t) = \langle Q_m(t) Q_n^* \rangle * K_{nn}^{-1}$, and, in particular,

$$G_{\mathbf{k}-\mathbf{q},\mathbf{q};\mathbf{k}}^{21}(t) = \frac{\langle Q_2(\mathbf{k}-\mathbf{q},\mathbf{q};t) \hat{A}_{-\mathbf{k}} \rangle}{\langle \hat{A}_{\mathbf{k}} \hat{A}_{-\mathbf{k}} \rangle}. \qquad (7)$$

Note that Eq. (6) is exact in the limit $t \to 0$ by construction of the basis set. Utilizing projection operator techniques [17,23,24] and cumulant expansion methods [16], the multiple-point correlation function $G_{\mathbf{k}-\mathbf{q},\mathbf{q};\mathbf{k}}^{21}(t)$ can be expressed in terms of two-point, two-time correlation functions as [15]

$$G_{\mathbf{k}-\mathbf{q},\mathbf{q};\mathbf{k}}^{21}(t) = \int_0^t G_{\mathbf{k}-\mathbf{q}}^{11}(t-\tau)$$

$$\times G_{\mathbf{q}}^{11}(t-\tau):\bar{M}_{\mathbf{k}-\mathbf{q},\mathbf{q};\mathbf{k}}^{21} \cdot G_{\mathbf{k}}^{11}(\tau)d\tau, \quad (8)$$

where $G_{\mathbf{k}}^{11}(t) = \langle \hat{A}_{\mathbf{k}}(t)\hat{A}_{-\mathbf{k}}\rangle/\langle \hat{A}_{\mathbf{k}}\hat{A}_{-\mathbf{k}}\rangle$ are the normalized, two-point and two-time correlation functions of the linear densities, and the ''vertices'' are given by

$$\bar{M}^{lm} = \left[\langle \dot{Q}_l Q_m^*\rangle - \int_0^\infty d\tau \langle \phi_l(\tau)\phi_m^*\rangle\right]K_{mm}^{-1}, \quad (9)$$

with the fluctuating force $\phi_l(t)$ defined by

$$\phi_l(t) \equiv e^{(1-\mathcal{P})\mathcal{L}t}(1-\mathcal{P})\dot{Q}_l, \quad (10)$$

where $\mathcal{L}$ is the Liouville operator.

Similarly, it can be shown that the three-time correlation function

$$G^{111}(t_1,t_2) = \langle Q_1(t_1+t_2)Q_1(t_1)Q_1^*\rangle \cdot K_{11}^{-1} \quad (11)$$

can be approximately written as [15]

$$G^{111}(t_2,t_1) = G^{11}(t_2)*\bar{M}^{111}*G^{111}(t_1)$$

$$+ G^{12}(t_2)*\bar{M}^{211}*G^{11}(t_1)$$

$$+ G^{11}(t_2)*\bar{M}^{112}*G^{21}(t_1)+O(N^{-1}), \quad (12)$$

where $\bar{M}^{lmn}$ is given by

$$\bar{M}^{lmn} = \langle Q_l Q_m Q_n^*\rangle \cdot K_{nn}^{-1}. \quad (13)$$

Furthermore, it was shown in Ref. [15] that $G^{12}(t_2)$ can be written in terms of the two-point, two-time functions and the $\bar{M}^{21}$ vertices in a manner analogous to Eq. (8).

The symmetry properties of the Hamiltonian can be used to greatly simplify the analysis of higher-order correlation functions. For example, since the Hamiltonian $\mathcal{H}$ is invariant under the transformation $\mathcal{TH}=\mathcal{H}$, where the self-adjoint time-reversal operator $\mathcal{T}$ acts on an arbitrary phase point $(\mathbf{r}^N,\mathbf{p}^N)$ by $\mathcal{T}(\mathbf{r}^N,\mathbf{p}^N)=(\mathbf{r}^N,-\mathbf{p}^N)$, all time correlation functions considered here have well-defined symmetry properties under $\mathcal{T}$, namely, $\mathcal{T}\hat{A}_{\mathbf{k}}^a = \gamma_a\hat{A}_{\mathbf{k}}^a$, where $\gamma_a=1$ for $a=N,H$ and $\gamma_a=-1$ for $a=T_1,T_2,L$. Furthermore, since the Liouville operator $\mathcal{L}$ transforms as $\mathcal{TL}=-\mathcal{LT}$, it is easy to show [15,25] that $\langle A_{\mathbf{k}}^a(t)A_{-\mathbf{k}}^b\rangle = \gamma_a\gamma_b\langle A_{\mathbf{k}}^a(-t)A_{-\mathbf{k}}^b\rangle$. It is straightforward to extend these arguments to multiple-time correlation functions for which $\langle A_{\mathbf{k}-\mathbf{q}}^a(t_1+t_2)A_{\mathbf{q}}^b(t_1)A_{-\mathbf{k}}^c\rangle = \gamma_a\gamma_b\gamma_c\langle A_{\mathbf{k}}^a(-t_1-t_2)A_{\mathbf{q}}^b(-t_1)A_{-\mathbf{k}}^c\rangle$.

A. Three-point correlations

We now turn our attention to evaluating the expressions for three-point correlation functions of three linear densities of the form in Eq. (6) for several different combinations of wave-vector and hydrodynamic labels in terms of the linear-

linear correlation functions $G^{11}(t)$. For simplicity, we consider correlation functions involving the transverse momentum mode $T_{2\mathbf{k}}$ henceforth abbreviated as just $T_{\mathbf{k}}$. From symmetry considerations it is easy to establish that the linear-linear correlation function $G_{\mathbf{k}}^{Ta}(t)=0$ unless $a=T$, which simplifies the subsequent analysis.

Looking first at the correlation function, $\langle T_{\mathbf{k}-\mathbf{q}}(t)T_{\mathbf{q}}(t)\hat{N}_{-\mathbf{k}}\rangle$, using Eq. (6) we have

$$\langle T_{\mathbf{k}-\mathbf{q}}(t)T_{\mathbf{q}}(t)\hat{N}_{-\mathbf{k}}\rangle = \frac{\langle \hat{N}_{\mathbf{k}}(t)\hat{A}_{-\mathbf{k}}^a\rangle}{\langle \hat{A}_{\mathbf{k}}^a\hat{A}_{-\mathbf{k}}^a\rangle}\langle \hat{A}_{-\mathbf{k}}^a T_{\mathbf{k}-\mathbf{q}}T_{\mathbf{q}}\rangle$$

$$+ G_{\mathbf{k}-\mathbf{q},\mathbf{q};\mathbf{k}}^{TT;N}(t)\langle \hat{N}_{\mathbf{k}}\hat{N}_{-\mathbf{k}}\rangle, \quad (14)$$

where the repeated index a is summed over the labels for N, T, L, and H, and

$$G_{\mathbf{k}-\mathbf{q},\mathbf{q};\mathbf{k}}^{TT;N}(t) \equiv \frac{\langle Q_2^{TT}(\mathbf{k}-\mathbf{q},\mathbf{q},t)\hat{N}_{-k}\rangle}{\langle \hat{N}_{\mathbf{k}}\hat{N}_{-\mathbf{k}}\rangle}.$$

The replacement of the ''21'' superscript in $G_{\mathbf{k}-\mathbf{q},\mathbf{q};\mathbf{k}}^{21}(t)$ by ''$TT;N$'' above is meant to denote the specific hydrodynamic labels under consideration. The semicolon separating the labels indicates that the labels ''TT'' correspond to the bilinear density, whereas the ''N'' labels the linear density in Eq. (7). Noting that $\langle \hat{A}_{-\mathbf{k}}^a T_{\mathbf{k}-\mathbf{q}}T_{\mathbf{q}}\rangle$ vanishes unless $a=N,H$, the first part of Eq. (14) can be written as

$$\frac{\langle \hat{N}_{\mathbf{k}}(t)\hat{N}_{-\mathbf{k}}\rangle}{S(k)}\langle \hat{N}_{-\mathbf{k}}T_{\mathbf{k}-\mathbf{q}}T_{\mathbf{q}}\rangle + \frac{\langle \hat{N}_{\mathbf{k}}(t)\hat{H}_{-\mathbf{k}}\rangle}{\langle N\rangle}\langle \hat{H}_{-\mathbf{k}}T_{k-\mathbf{q}}T_{\mathbf{q}}\rangle$$

$$= \frac{m}{\beta}\langle \hat{N}_{\mathbf{k}}(t)\hat{N}_{-\mathbf{k}}\rangle - \frac{2m}{\sqrt{6}\beta}\langle \hat{N}_{\mathbf{k}}(t)\hat{H}_{-\mathbf{k}}\rangle,$$

where $S(k)=\langle \hat{N}_{\mathbf{k}}\hat{N}_{-\mathbf{k}}\rangle$ is the static structure factor. The normalized multiple-point correlation function $G_{\mathbf{k}-\mathbf{q},\mathbf{q};\mathbf{k}}^{TT;N}(t)$ of the basis set variable Q_2^{TT} can be evaluated using Eq. (8),

$$G_{\mathbf{k}-\mathbf{q},\mathbf{q};\mathbf{k}}^{TT;N}(t) = \int_0^t G_{\mathbf{k}-\mathbf{q}}^{TT}(t-\tau)G_{\mathbf{q}}^{TT}(t-\tau)$$

$$\times \bar{M}_{\mathbf{k}-\mathbf{q},\mathbf{q};\mathbf{k}}^{TT;a}G_{\mathbf{k}}^{aN}(\tau)d\tau, \quad (15)$$

where a is summed over the labels N and H only since the $\bar{M}^{TT;a}$ vertex vanishes when $a=L$ or T. The explicit form of the vertex is given by Eq. (9), which involves a ''Euler part''

$$\frac{\langle \dot{Q}_{\mathbf{k}-\mathbf{q},\mathbf{q}}^{TT}\hat{A}_{-\mathbf{k}}^a\rangle}{\langle \hat{A}_{\mathbf{k}}^a\hat{A}_{-\mathbf{k}}^a\rangle}$$

and a dissipative part

$$-\int_0^\infty d\tau \langle \phi_{\mathbf{k}-\mathbf{q},\mathbf{q}}^{TT}(\tau)\phi_{-\mathbf{k}}^a\rangle/\langle \hat{A}_{\mathbf{k}}^a\bar{A}_{-\mathbf{k}}^a\rangle.$$

These contributions to the vertex can be evaluated as detailed in the Appendix, and one finds that to leading order in the wave vector, only the $a=L$ term contributes at order k (with corrections of order k^3), whereas the other vertex with $a=H$ gives a contribution proportional to k^2. Putting all this together, we obtain the expression

$$\langle T_{\mathbf{k}-\mathbf{q}}(t)T_{\mathbf{q}}(t)\hat{N}_{-\mathbf{k}}\rangle = \frac{m}{\beta}\langle\hat{N}_{\mathbf{k}}(t)\hat{N}_{-\mathbf{k}}\rangle - \frac{2m}{\sqrt{6}\beta}\langle\hat{N}_{\mathbf{k}}(t)\hat{H}_{-\mathbf{k}}\rangle$$

$$+ G^{TT;N}_{\mathbf{k}-\mathbf{q},\mathbf{q};\mathbf{k}}(t)\langle\hat{N}_{\mathbf{k}}\hat{N}_{-\mathbf{k}}\rangle, \qquad (16)$$

where

$$G^{TT;N}_{\mathbf{k}-\mathbf{q},\mathbf{q};\mathbf{k}}(t)=\int_0^t G^{TT}_{\mathbf{k}-\mathbf{q}}(t-\tau)G^{TT}_{\mathbf{q}}(t-\tau)\bar{M}^{TT;L}_{\mathbf{k}-\mathbf{q},\mathbf{q};\mathbf{k}}G^{LN}_{\mathbf{k}}(\tau)d\tau$$

$$+\int_0^t G^{TT}_{\mathbf{k}-\mathbf{q}}(t-\tau)G^{TT}_{\mathbf{q}}(t-\tau)$$

$$\times\bar{M}^{TT;H}_{\mathbf{k}-\mathbf{q},\mathbf{q};\mathbf{k}}G^{HN}_{\mathbf{k}}(\tau)d\tau, \qquad (17)$$

and the functions $G^{TT}_{\mathbf{k}}(\tau)$, $G^{LN}_{\mathbf{k}}(\tau)$, and $G^{HN}_{\mathbf{k}}(\tau)$ are given explicitly by

$$G^{TT}_{\mathbf{k}}(\tau)=\langle T_{\mathbf{k}}(\tau)T_{-\mathbf{k}}\rangle/m\langle N\rangle k_BT,$$

$$G^{LN}_{\mathbf{k}}(\tau)=\langle L_{\mathbf{k}}(\tau)\hat{N}_{-\mathbf{k}}\rangle/S(k),$$

$$G^{HN}_{\mathbf{k}}(\tau)=\langle H_{\mathbf{k}}(\tau)\hat{N}_{-\mathbf{k}}\rangle/S(k).$$

The vertices $\bar{M}^{TT;L}_{\mathbf{k}-\mathbf{q},\mathbf{q};\mathbf{k}}$ and $\bar{M}^{TT;H}_{\mathbf{k}-\mathbf{q},\mathbf{q};\mathbf{k}}$ are given in the Appendix. Note that if the dissipative parts of the vertices are neglected, only the first time-convolution integral in Eq. (17) contributes to $\langle T_{\mathbf{k}-\mathbf{q}}(t)T_{\mathbf{q}}(t)\hat{N}_{-\mathbf{k}}\rangle$.

From similar considerations, it is not difficult to obtain expressions for other correlation functions. For example, we find that the multiple-point functions $\langle T_{\mathbf{k}-\mathbf{q}}(t)L_{\mathbf{q}}(t)T_{-\mathbf{k}}\rangle$ and $\langle T_{\mathbf{k}-\mathbf{q}}(t)\hat{N}_{\mathbf{q}}(t)T_{-\mathbf{k}}\rangle$ are given by

$$\langle T_{\mathbf{k}-\mathbf{q}}(t)L_{\mathbf{q}}(-\mathbf{k})\rangle=G^{TL;T}_{\mathbf{k}-\mathbf{q},\mathbf{q};\mathbf{k}}(t), \qquad (18)$$

$$\langle T_{\mathbf{k}-\mathbf{q}}(t)\hat{N}_{\mathbf{q}}(t)T_{-\mathbf{k}}\rangle=\frac{S(q)}{\langle N\rangle}\langle T_{\mathbf{k}}(t)T_{-\mathbf{k}}\rangle+G^{TN;T}_{\mathbf{k}-\mathbf{q},\mathbf{q};\mathbf{k}}(t) \qquad (19)$$

with

$$G^{TL;T}_{\mathbf{k}-\mathbf{q},\mathbf{q};\mathbf{k}}(t)=\int_0^t G^{TT}_{\mathbf{k}-\mathbf{q}}(t-\tau)\sum_{\alpha=L,N,H}G^{L\alpha}_{\mathbf{q}}(t-\tau)$$

$$\times\bar{M}^{T\alpha;T}_{\mathbf{k}-\mathbf{q},\mathbf{q};\mathbf{k}}G^{TT}_{\mathbf{k}}(\tau)d\tau \qquad (20)$$

and

$$G^{TN;T}_{\mathbf{k}-\mathbf{q},\mathbf{q};\mathbf{k}}(t)=\int_0^t G^{TT}_{\mathbf{k}-\mathbf{q}}(t-\tau)\sum_{a=L,N,H}G^{Na}_{\mathbf{q}}(t-\tau)$$

$$\times\bar{M}^{Ta;T}_{\mathbf{k}-\mathbf{q},\mathbf{q};\mathbf{k}}G^{TT}_{\mathbf{k}}(\tau)d\tau. \qquad (21)$$

In Eqs. (20) and (21), to leading order in the wave vectors, the vertex $\bar{M}^{TL;T}$ for $a=L$ contributes at Euler order and is imaginary, while the vertices $\bar{M}^{TN;T}$ and $\bar{M}^{TN;T}$ contribute at dissipative order and are real. However, since $G^{LL}_{\mathbf{q}}(t-\tau)$, $G^{NN}_{\mathbf{q}}(t-\tau)$, $G^{HN}_{\mathbf{q}}(t-\tau)$, and $G^{NH}_{\mathbf{q}}(t-\tau)$ are real and $G^{LN}_{\mathbf{q}}(t-\tau)$, $G^{NL}_{\mathbf{q}}(t-\tau)$, and $G^{LH}_{\mathbf{q}}(t-\tau)$ are purely imaginary by time-reversal symmetry, the correlation functions $G^{TT;N}_{\mathbf{k}-\mathbf{q},\mathbf{q};\mathbf{k}}(t)$ and $G^{TN;T}_{\mathbf{k}-\mathbf{q},\mathbf{q};\mathbf{k}}(t)$ are real whereas $G^{TL;T}_{\mathbf{k}-\mathbf{q},\mathbf{q};\mathbf{k}}(t)$ is purely imaginary. Note that at $t=0$, the expressions for the functions G^{21} in Eqs. (17), (21), and (20) vanish and the multiple-point correlation functions are given exactly.

B. Three-time correlations

The three-time correlation functions

$$G^{TLT}_{\mathbf{k}-\mathbf{q},\mathbf{q},\mathbf{k}}(t_1,t_2)=\frac{\langle T_{\mathbf{k}-\mathbf{q}}(t_1+t_2)L_{\mathbf{q}}(t_1)T_{-\mathbf{k}}\rangle}{\langle N\rangle mk_BT},$$

$$G^{TNT}_{\mathbf{k}-\mathbf{q},\mathbf{q},\mathbf{k}}(t_1,t_2)=\frac{\langle T_{\mathbf{k}-\mathbf{q}}(t_1+t_2)\hat{N}_{\mathbf{q}}(t_1)T_{-\mathbf{k}}\rangle}{\langle N\rangle mk_BT}$$

can be evaluated in a straightforward fashion using the results of the preceding section. In Ref. [15], it was shown that the multiple-time vertices $\bar{M}^{lmn}$ reduce to very simple forms to leading N order, with corrections of order $M/N\sim k_ca\approx10^{-5}$ for systems of moderate density [17]. Using the reduced forms of $\bar{M}^{211}$ and $\bar{M}^{112}$ and Eq. (12), the leading N-order expressions for these multiple-time functions are

$$G^{TLT}_{\mathbf{k}-\mathbf{q},\mathbf{q},\mathbf{k}}(t_1,t_2)=G^{T;TL}_{\mathbf{k}-\mathbf{q};\mathbf{k},-\mathbf{q}}(t_2)\langle L_{\mathbf{q}}L_{-\mathbf{q}}\rangle G^{TT}_{\mathbf{k}}(t_1)$$

$$+G^{TT}_{\mathbf{k}-\mathbf{q}}(t_2)G^{TL;T}_{\mathbf{k}-\mathbf{q},\mathbf{q};\mathbf{k}}(t_1) \qquad (22)$$

and

$$G^{TNT}_{\mathbf{k}-\mathbf{q},\mathbf{q},\mathbf{k}}(t_1,t_2)=G^{TT}_{\mathbf{k}-\mathbf{q}}(t_2)\frac{S(q)}{\langle N\rangle}G^{TT}_{\mathbf{k}}(t_1)$$

$$+G^{T;TN}_{\mathbf{k}-\mathbf{q};\mathbf{k},-\mathbf{q}}(t_2)S(q)G^{TT}_{\mathbf{k}}(t_1)$$

$$+G^{TT}_{\mathbf{k}-\mathbf{q}}(t_2)G^{TN;T}_{\mathbf{k}-\mathbf{q},\mathbf{q};\mathbf{k}}(t_1). \qquad (23)$$

Using the symmetry properties of $G^{lm}(t)$ [15], one can write $G^{T;Ta}(t)\langle\hat{A}^a\hat{A}^{a*}\rangle=[G^{Ta;T}(-t)]^*$; and Eqs. (22) and (23) can be expressed in terms of $G^{21}(t)$ alone as

$$G^{TLT}_{\mathbf{k}-\mathbf{q},\mathbf{q},\mathbf{k}}(t_1,t_2)=-G^{TL;T}_{-\mathbf{k},\mathbf{q};\mathbf{q}-\mathbf{k}}(t_2)G^{TT}_{\mathbf{k}}(t_1)$$

$$+G^{TT}_{\mathbf{k}-\mathbf{q}}(t_2)G^{TL;T}_{\mathbf{k}-\mathbf{q},\mathbf{q};\mathbf{k}}(t_1) \qquad (24)$$

and

$$G^{TNT}_{\mathbf{k}-\mathbf{q},\mathbf{q},\mathbf{k}}(t_1,t_2)=G^{TT}_{\mathbf{k}-\mathbf{q}}(t_2)\frac{S(q)}{\langle N\rangle}G^{TT}_{\mathbf{k}}(t_1)$$

$$+G^{TN;T}_{-\mathbf{k},\mathbf{q};\mathbf{q}-\mathbf{k}}(t_2)G^{TT}_{\mathbf{K}}(t_1)$$

$$+G^{TT}_{\mathbf{k}-\mathbf{q}}(t_2)G^{TN;T}_{\mathbf{k}-\mathbf{q},\mathbf{q};\mathbf{k}}(t_1), \qquad (25)$$

where the time-reversal symmetry properties and the behavior under complex conjugation of the $G^{21}(t)$ correlation functions has been used.

In Sec. IV, these expressions will be compared to results from simulations of a hard-sphere system at moderate density.

III. SIMULATION METHOD

The dynamics of hard spheres consist of free, rectilinear motion until the distance between two spheres (i and j) becomes equal to their diameter a, at which point an instantaneous collision takes place, leading to the momentum changes

$$\mathbf{p}_i \rightarrow \mathbf{p}_i - \hat{\sigma}[(\mathbf{p}_i - \mathbf{p}_j) \cdot \hat{\sigma}],$$

$$\mathbf{p}_j \rightarrow \mathbf{p}_j + \hat{\sigma}[(\mathbf{p}_i - \mathbf{p}_j) \cdot \hat{\sigma}],$$

where the collision normal $\hat{\sigma}$ equals $(\mathbf{r}_j - \mathbf{r}_i)/a$ at contact.

Due to the simplicity of the equations of motion, the dynamical evolution of the hard-sphere system can be computed exactly using an event-driven procedure in which one calculates the first possible collision of all spheres under the assumption that no other particles collide. The phase point of the system is then evolved up to the time of the earliest of these collisions, and the process is repeated until the total desired run time is completed.

Without additional bookkeeping, the number of spheres with which a specific particle can collide is $N-1$, and hence $O(N)$ calculations of collision times are required for each particle after it collides. As the number of collisions per unit time is extensive, the simulation time scale increases quadratically with the number of particles. Considerable improvements in simulation efficiency can be gained using a division of the system into regions (called cells) and data structures to optimize the search for the next collision time [26].

To use the cell structure in a simulation, the system of dimension $L_x \times L_y \times L_z$ is divided into an integer number of cells of dimension $l_x \times l_y \times l_z$, where each of the lengths l_x, l_y, and l_z is no smaller than the diameter of the hard spheres. Now, in addition to the collision events between spheres, the cell in which each sphere is located and the time at which the particle will leave its cell is recorded. This is advantageous because the number of spheres that can collide with a given sphere before a particle moves out of its cell is proportional to the number of spheres in its vicinity, i.e., the spheres in the same cell or in one of the 26 neighboring cells. Using the cell structures, the number of spheres within the vicinity of a given particle is of order $O(l_x l_y l_z N / L_x L_y L_z) = O(1)$, provided the lengths of each cell are of the order of the diameter of the particles, and hence far fewer collision times of pairs of particles must be computed after each collision event. However, the use of cells comes at the cost of increasing the complexity of the event-driven simulation since after a crossing event for a given particle, the collision times of the given sphere with spheres that previously were not in its vicinity must be considered, and, if necessary, the first stored collision event adjusted. In addition, the next crossing time in the same direction is recalculated. Similarly, after a collision event between two particles, new collisions within the same cell, as well as the new cell-crossing times must be calculated for the particles involved in the event.

Even though the calculations after a crossing or a collision event are of $O(1)$ when many cells are used, it is still necessary to search the event list of each sphere to find the earliest event in the simulation. If the spheres are simply stored in a linear array, this implies a look-up time that scales linearly with N, and the algorithm scales as N^2 as before, though with a considerably lower prefactor than without the cell structure. If, on the other hand, the spheres are stored in a binary tree, ordered according to their first event, the search for the first event scales as the logarithm of the number of elements, which in our implementation is N. Deleting an element from the tree is an $O(1)$ operation, while the insertion of new elements into the tree requires a tree search, which scales as $\ln N$. Since the number of crossing and collision events is extensive, the algorithm scales as $N \ln N$, and the overall speed up of the algorithm over a simple event-based simulation behaves as $N / \ln N$. It should be noted, however, that the cell structure reduces the number of collisions to be considered to a large extent, so the prefactor is also quite reduced.

There is some flexibility in selecting the size of the cells to be used in the simulation. Larger cells require fewer crossing times to be calculated at the expense of increasing the number of collisions, which must be computed within each cell. As Rapaport has noted [26], the optimal choice of the dimensions of the cell for systems of low density is intermediate between the size of the full system and the diameter of the hard spheres, whereas the smallest possible cells make for the fastest simulation for higher densities. In the simulations reported in the following section, the optimal length of cells was found to correspond roughly with the diameter of the hard-sphere particles.

IV. RESULTS AND DISCUSSION

In this section, the mode-coupling expressions for the higher-order correlations functions given in Sec. II are compared to those obtained from event-based molecular dynamics simulations in the microcanonical ensemble at an inverse temperature $\beta = 3$. The size of the periodic system in the simulation was chosen to be $L_x = L_y = L_z = 15.7526$, such that for $N = 1382$ hard-sphere particles of diameter $a = 1$, the reduced density $\rho^* = 0.25$ (ρ / ρ_c, where ρ_c is the density at close packing) and the magnitude of the smallest wave vector $k_0 a = 2 \pi a / L_x = 0.398\,867$ coincide with one of the cases in Ref. [27]. A total number of $15^3 = 3375$ cells were used, leading to a collision rate (including data collection) of roughly $3.2 \times 10^6 \, \mathrm{h}^{-1}$ on a 600-MHz digital 21164 processor. The event-dynamics simulations were run on nine nodes of a 30-node "Beowulf" cluster for a total of 4100 CPU hours, where each node carried out 3750 short molecular dynamics trajectories of approximately 403 500 collisions. The initial configuration of the system for each of the individual runs was randomly chosen using a simple rejection method. In all results reported below, time is expressed in dimensionless

units t/t_c, where t_c is the mean collision time calculated from the simulation. At the density and temperature of the simulation, the mean collision time is roughly half the time t_m it takes a particle to move over a distance equal to its diameter a ($t_c/t_m \approx 0.412$).

To evaluate time correlation functions in the simulation, the values of the linear densities $A_{\mathbf{k}}(t)$ were calculated for a set of wave vectors at $M+1$ fixed time intervals $t=0$, Δt, $2\Delta t,...$ and stored in an array $A[k][i]$, where the index k runs over the wave-vector indices and i runs from 0 to M. In all molecular dynamics runs, the time interval $\Delta t/t_m = 0.15$ and $M=400$. Two-point, two-time correlation functions for a given time interval were accumulated on the fly by storing the product of accumulated arrays $A[k][(t/\Delta t)(\mathrm{mod}\,M)] \times A^*[k]([(t-s)/\Delta t](\mathrm{mod}\,M))$ in an array for the correlation function $\langle A_k(s)A_k^* \rangle$ for all relevant values of s. At the end of the run the result was divided by the number of points accumulated. Multiple-point and multiple-time correlation functions are evaluated in an analogous fashion.

Good statistics are difficult to obtain for the higher-order correlation functions since the functions are the average of a product of multiple factors of the linear densities $A_{\mathbf{k}}$. For example, the three-point correlation functions are constructed by averages of quantities that are typically of the order of N^3, whereas the final average itself is of $O(N)$. In order to optimize the sampling, many relatively short runs of duration $R=4M\Delta t$ were performed and averaged on the fly. The strategy of using many short runs seems to be better than the alternative of performing a single long run of equal total length perhaps because it reduces the effect of abnormally large points that contaminate the signal for a long time.

Further improvement of the statistics of the calculated correlation functions is possible by exploiting the isotropy of the system. To simplify the comparison between theoretical predictions and the simulation results, all wave vectors were taken to be co-linear along the $\hat{x}$ axis so that $\mathbf{k} \cdot \mathbf{q} = kq$, where $k=|\mathbf{k}|$ and $q=|\mathbf{q}|$. Since the wave vectors $\mathbf{k}$ and $\mathbf{q}$ are parallel, the quantities $\langle A_{k\hat{x}-q\hat{x}}(t)A_{q\hat{x}}(t)A_{k,\hat{x}}^* \rangle$, $\langle A_{k\hat{y}-q\hat{y}}(t)A_{q\hat{y}}(t)A_{k,\hat{y}}^* \rangle$, and $\langle A_{k\hat{z}-q\hat{z}}(t)A_{q\hat{z}}(t)A_{k,\hat{z}}^* \rangle$, can be computed from the simulation in a periodic, cubic simulation box and averaged to obtain improved statistics. In addition, for many of the correlation functions considered here, such as $\langle T_{k-q}(t)N_q(t)T_k^* \rangle$, the number of points used to calculate the higher-order correlation functions can be effectively doubled by averaging over the transverse directions $\hat{y}$ and $\hat{z}$.

The estimation of statistical uncertainty in the simulation data is problematic as it involves constructing an autocorrelation function for each point measured in the time-correlation function [28]. Such a procedure is both memory and computationally intensive, and slows down the simulation dramatically. In fact, most of the computational time of the simulation is spent accumulating data and calculating the correlation functions rather than performing the molecular dynamics. We therefore adopt a simpler approach to estimate the error using the symmetry properties of the correlation functions. From reflection symmetry, it follows that all correlation functions are either real or imaginary [15]. For a real correlation function, the imaginary part vanishes and hence

the imaginary part calculated from the simulation gives a rough estimate of the error in the real part, as both are calculated from the same configurations and involve terms of similar structure. To approximate the statistical uncertainty for a real correlation function, a histogram of the values of the imaginary part is constructed to determine the interval of values containing 96% of the points. The size of this interval provides an estimate of the error in the real part, taken to be constant for all times of the correlation function. Such an approximation seems reasonable given that the variations in the imaginary part in the simulations are observed to be relatively constant over the total time interval $M\Delta t$. For an imaginary correlation function, the analogous procedure is done using the variations in the real part.

The simulation results for the two-point, two-time correlation functions were checked against generalized Enskog theory results [27]. The statistical uncertainty in the normalized correlation functions (as obtained by the procedure above) are quite small (of the order of 0.001). The numerical value for the shear viscosity, extracted from the exponential decay of the autocorrelation function of the transverse velocity $T_{\mathbf{k}}$, was compared to the kinetic theory prediction for this quantity [21] and excellent agreement was observed.

The time-convolution integrals in the mode-coupling expressions for the higher-order correlation functions were evaluated by numerically integrating data for the two-point, two-time correlation functions $G_k^{ab}(t)$ obtained directly from the simulation. Since the error bars of the $G_k^{ab}(t)$ are very small, the level of uncertainty in the theoretical prediction for the higher-order correlation functions is negligible in comparison to the uncertainty in the simulation data for the higher-order correlation function. Furthermore, no significant differences were noted in the convolution integrals calculated using the simulation data and calculated from high quality functional fits of the integrands. In principle, one could also use the hydrodynamic forms for all two-point, two-time correlation functions in combination with an accurate equation of state and kinetic theory results for the transport coefficients, but since the simple correlation functions were obtained with great accuracy in the simulation, the actual data was used.

As described in the Appendix, the dissipative part of the vertices for $\bar{M}^{TN;T}$, $\bar{M}^{TH;T}$, and $\bar{M}^{TT;H}$ have free parameters v_n, v_h, and v_{th}, which must be fitted to the data if the dissipative contributions are to be included in the predictions for both the multiple-point and multiple-time correlation functions. In practice, this is accomplished by selecting particular wave-vector magnitudes k and q and fitting the parameters according to the simulation results. This procedure is illustrated in Fig. 1 for the multiple-point correlation function

$$C^{TL;T}(t) = \langle T_{k-q}(t)L_q(t)T_{-k} \rangle / \langle N \rangle m k_B T$$

for wave vectors $k=k_0$ and $q=2k_0$. Note that although the dissipative contribution to the overall correlation function in Eq. (20) depends on the two parameters v_n (n coupling) and v_h (h coupling), these parameters can be uniquely determined since the asymptotic time behavior is determined en-
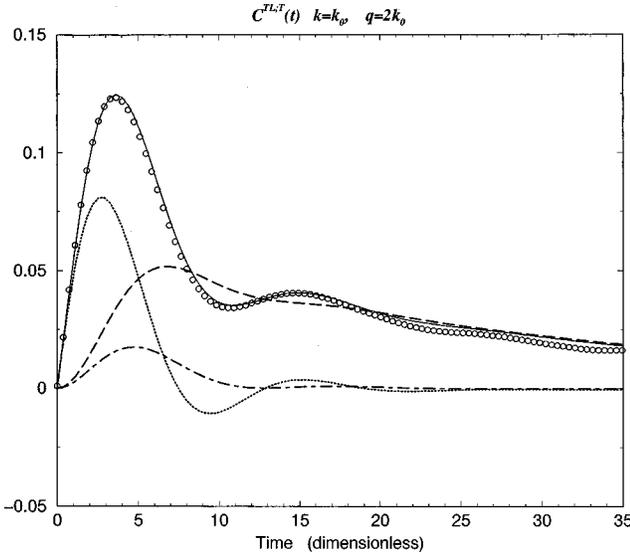
FIG. 1. The fitting procedure for the three-point correlation function $C^{TL;T}(t)$ for the wave vectors $k=k_0$, $q=2k_0$, where $k_0 a = 0.398\,867$. The unconnected circles are the simulation results, the solid line denotes the full mode-coupling results, the dotted line denotes the mode-coupling results with Euler vertices, and the long-dashed and dot-dashed lines represent the contributions from the n-dissipative and h-dissipative vertices, respectively. For clarity, the statistical uncertainties in all quantities have been omitted.

FIG. 2. The correlation functions $C^{TT;N}(t)$ (left panels) and $C^{TL;T}(t)$ (right panels) as a function of reduced time at various wave vectors. In the top row, the wave-vector arguments are $k=k_0, q=2k_0$ [open unconnected circles, simulation results; solid line, mode-coupling theory (MCT) prediction] and $k=2k_0, q=k_0$ (open unconnected squares, simulation results; dotted line, MCT prediction). In the middle row, the wave-vector arguments are $k=k_0$, $q=3k_0$ (open unconnected circles, simulation results; solid line, MCT prediction) and $k=3k_0, q=k_0$ (open unconnected squares, simulation results; dotted line, MCT prediction). In the bottom row, the wave-vector arguments are $k=2k_0, q=3k_0$ (open unconnected circles, simulation results; solid line, MCT prediction) and $k=3k_0, q=2k_0$ (open unconnected squares, simulation results; dotted line, MCT prediction). For clarity, the statistical uncertainties in all quantities have been omitted.

tirely by the n-coupling contribution. Once this parameter is set (here, $v_n = -0.18$), v_h can be determined by fitting the height of the first peak (found to be $v_h = 0.90$). A similar procedure is used for the $\bar{M}^{TT;H}$ vertex in Eq. (17), which is relevant for the correlation function

$$C^{TT;N}(t) = \langle T_{k-q}(t) T_q(t) \hat{N}_{-k} \rangle / S(k),$$

and it is found that $v_{th} = -0.62$. Note that it is, in fact, the additional couplings, which arise at dissipative order, that account for the slow decay of the three-point correlation function in Fig. 1. It is therefore quite apparent that ordering of terms using the wave vector must be done carefully for the system under consideration, since contributions that appear at higher orders of the wave vector can actually dominate lower-order terms.

With the coupling parameters fixed by the fitting procedure, one can then compare the simulation results with the theoretical predictions for arbitrary wave-vector combinations. In Fig. 2, the simulation and theoretical predictions for the multiple-point correlation functions $C^{TL;T}(t)$ and $C^{TT;N}(t)$ are shown as functions of time for a number of wave-vector combinations. The remarkable agreement between the simulation results and the theoretical predictions of both three-point correlation functions over all time regimes and wave-vector combinations is a clear indication that the formulation of the mode-coupling theory is sound.

It is interesting to see how the theoretical predictions of the present formalism compare to those obtained from a mode-coupling theory in which Gaussian statistical behavior is assumed in the multilinear basis set. This type of assump-

tion roughly corresponds to Kawasaki's original formulation of mode-coupling theory [18], which is based upon a nonlinear Langevin equation with Gaussian noise (or fluctuating forces). Such a Gaussian theory for the multiple-point correlation functions differs from the present formulation in two significant ways: First, since the subtractions in the multilinear basis set [see Eq. (3)] involve static three-point correlation functions of the linear densities, which vanish under the assumption of Gaussian statistics, the Gaussian theory neglects terms of the form

$$\langle \hat{A}_{\mathbf{k}}(t) \hat{A}_{-\mathbf{k}} \rangle \cdot K_{11}^{-1} \cdot \langle \hat{A}_{-\mathbf{k}} \hat{A}_{\mathbf{k}-\mathbf{q}} \hat{A}_{\mathbf{q}} \rangle,$$

which appear, for instance, in the mode-coupling expression for $C^{TT;N}(t)$. These terms make an important contribution to the multiple-point correlations functions on all time scales, and particularly for short times. Second, since the subtraction terms vanish in the Gaussian theory, the coupling vertices are significantly affected. For example, looking at the Euler order contributions to the vertex $\bar{M}^{TT;N}$, the vertex in the Gaussian approximation becomes $V^{TT;N}$ according to

$$\bar{M}^{TT;N} = \langle \dot{Q}^{TT}_{k-q,q} \hat{N}_{-k} \rangle / S(k) = \langle (T_{k-q} T_q) \hat{N}_{-k} \rangle / S(k) \equiv V^{TT;N}. \tag{26}$$

TABLE I. Expressions for the leading behavior of the *Euler* vertices $\bar{M}^{21}$ and their Gaussian counterparts V^{21}.

	$TL;T$	$TT;L$
$M^{21}_{\mathbf{k-q,q;k}}$	$ik\beta^{-1}$	$i\frac{2}{3}kp/\rho$
$V^{21}_{\mathbf{k-q,q;k}}$	$ik\beta^{-1}$	$-ik\beta^{-1}$

Similar differences between the vertices V in the Gaussian approximation and the $\bar{M}$ vertices appear in the dissipative parts of the $\bar{M}^{TN;T}$ and $\bar{M}^{TH;T}$ (see Tables I and II).

In order to assess how each of these differences affects three-point correlation functions, we once again consider the correlation functions $C^{TT;N}(t)$ and $C^{TL;T}(t)$. The first correlation function differs not only in the explicit form of the coupling vertices but also in the form of the expressions due to the subtraction terms in the basis set. The second correlation function, on the other hand, vanishes at $t=0$ by symmetry and does not contain contributions that are directly proportional to two-point, two-time correlation functions [see Eq. (18)]. For this correlation function, the differences between the Gaussian and full mode-coupling theory arise solely due to differences between the Gaussian vertices $V^{TN;T}$, $V^{TH;T}$ and their full counterparts. In Fig. 3, the Gaussian and full mode-coupling expressions are compared to the simulation data for the wave vectors $k=k_0$, $q=3k_0$. From these plots, it is clear that the Gaussian theory poorly predicts the time dependence of $C^{TT;N}(t)$ on all time scales and also gives worse results for the correlation function $C^{TL;T}(t)$. Similar behavior can be seen for other wave-vector combinations.

Turning now to the multiple-time correlation functions, the simulation results and theoretical predictions for the multiple-time correlation functions $G^{TLT}(t_1,t_2)$ and $G^{TNT}(t_1,t_2)$ for several different wave vectors are plotted in Fig. 4 as a function of time t for the time combinations (t_1,t_2) of (t,t), $(t,3t)$, and $(3t,t)$. The excellent agreement between the full mode-coupling theory and simulation results strongly suggests that the assumptions discussed at length in Ref. [15], of what determines whether a correlation function decays quickly or not, are appropriate. These assumptions are necessary to obtain mode-coupling equations that are local in time.

Note that the time symmetry properties are evident in the two graphs in the first row of Fig. 4, which correspond to the wave vectors $k=k_0$, $q=2k_0$. For these wave vectors, the time symmetries can be obtained by noting that

$$\langle T_{k-q}(t_1+t_2)A_q^a(t_1)T_{-k}\rangle = \langle T_{k-q}(t_2)A_q^a T_{-k}(-t_1)\rangle,$$

FIG. 3. The full mode-coupling theory (MCT), Gaussian MCT, Euler-order MCT predictions, and simulation data for the correlation functions $C^{TT;N}(t)$ (left panel) and $C^{TL;T}(t)$ (right panel) at wave vectors $k=k_0$ and $q=3k_0$. In both panels, the unconnected circles are the simulation data, the solid, dotted, and dashed lines represent the full MCT, the Euler-order MCT, and the Gaussian MCT results, respectively. The error estimates represent 96% confidence intervals. Note that the Gaussian MCT theory is qualitatively incorrect on all time scales for $C^{TT;N}(t)$.

since the equilibrium distribution function is stationary. Inverting all time arguments and using the properties of the densities under time reversal, one obtains

$$\langle T_{k-q}(t_2)A_q^a T_{-k}(-t_1)\rangle = \gamma_a\langle T_{k-q}(-t_2)A_q^a T_{-k}(t_1)\rangle,$$

where $\gamma_a=1$ for $a=N$, H and $\gamma_a=-1$ for T,L. When $k-q=-k$, we find that

$$\langle T_{-k}(t_1+t_2)L_{2k}(t_1)T_{-k}\rangle = -\langle T_{-k}(t_1+t_2)L_{2k}(t_2)T_{-k}\rangle,$$

which implies that this correlation function is antisymmetric under interchange of t_1 with t_2 (and therefore vanishes when $t_1=t_2$), while $\langle T_{-k}(t_1+t_2)L_{2k}(t_1)T_{-k}\rangle$ is symmetric under the exchange of t_1 and t_2. It is reassuring, though not surprising, that the mode-coupling theory respects these time-reversal properties.

One may also calculate the multiple-time correlation functions via Eqs. (24) and (25) using the simulation data for the multiple-point functions $G^{TN;T}$ and $G^{TL;T}$. However, since the mode-coupling results for these functions are already in excellent agreement with the simulation data, the improvement obtained using the simulation results for the G^{21} is generally statistically negligible. Furthermore, the simulations to calculate the multiple-point functions are computationally intensive compared to calculations of the two-point functions. It is therefore far easier to generate predictions with small statistical uncertainties using the mode-coupling theory expressions for the multiple-point functions.

TABLE II. Expressions for leading behavior of the *dissipative* vertices $\bar{M}^{21}$ and their Gaussian counterparts V^{21}. Note that in the table k and q stand for the x component of $\mathbf{k}$ and $\mathbf{q}$, respectively.

	$TH;T$	$TN;T$	$TT;H$
$M^{21}_{\mathbf{k-q,q;k}}$	$-k(k-q)[v_h - \sqrt{\frac{2}{3}}\,\eta/m\rho]$	$-k(k-q)v_n + k^2 S(q)\eta/m\rho$	$-k^2[v_{th} + (4m/2\sqrt{6\beta})(\lambda/k_B)]$
$V^{21}_{\mathbf{k-q,q;k}}$	$-k(k-q)v_h - k_q\eta/m\rho$	$-k(k-q)v_n$	$-k^2 v_{th}$
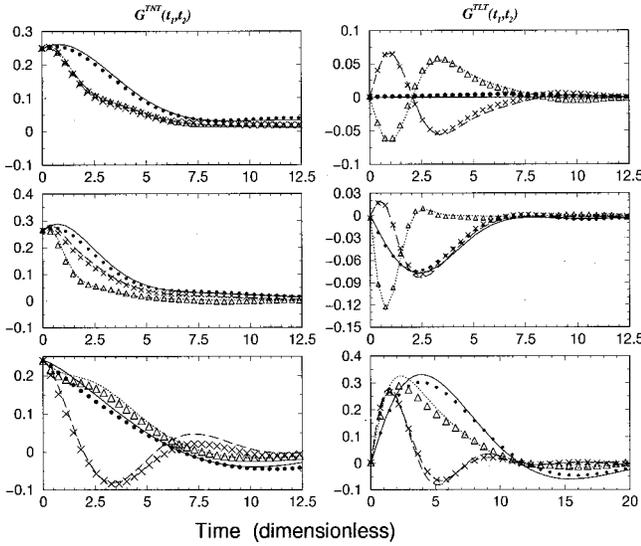
FIG. 4. The multiple-time correlation functions $G^{TNT}(t_1,t_2)$ and $G^{TLT}(t_1,t_2)$ as a function of reduced time for various wave-vector combinations. In all panels, the unconnected dots, crosses, and triangles correspond to the simulation results for the time arguments $t_1=t,t_2=t$, $t_1=3t,t_2=t$, and $t_1=t,t_2=3t$, respectively. The solid, dashed, and dotted lines correspond to the respective mode-coupling predictions. The results in the top, middle, and bottom rows are for the wave-vector arguments $k=k_0,q=2k_0$, $k=k_0$, $q=3k_0$, and $k=2k_0,q=k_0$. For clarity, the statistical uncertainties in all quantities have been omitted.

Since the mode-coupling formalism relates the multiple-time correlation functions to multiple-point correlation functions, the deficiencies in the Gaussian theory for the three-point functions are carried over to the predictions for three-time functions. This point is confirmed by the difference in the behavior of the Gaussian versus full mode-coupling theory results for the multiple-time correlation functions shown in Fig. 5. Once again, the Gaussian theory predictions
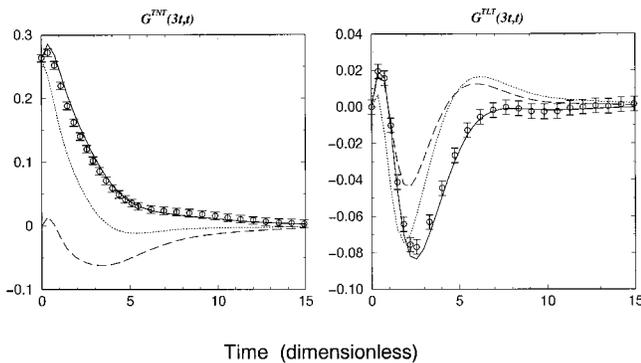
FIG. 5. The full mode-coupling theory (MCT), Euler-order MCT, and Gaussian MCT predictions and simulation data for the multiple-time correlation functions $G^{TNT}(t_1,t_2)$ (left panel) and $G^{TLT}(t_1,t_2)$ (right panel) at wave vectors $k=k_0$ and $q=3k_0$ and time arguments $t_1=3t,t_2=t$. In both panels, the unconnected circles are the simulation data, the solid, dotted, and dashed lines represent the full MCT theory, the Euler MCT, and the Gaussian MCT results, respectively. The error estimates represent 96% confidence intervals.

for multiple-time correlations are qualitatively incorrect on all time scales, and particularly so for correlation functions that do not vanish when $t_1=t_2=0$. Furthermore, as might be expected from the discussion above of the dissipative contribution to the three-point correlation functions, the inclusion of the additional couplings arising at dissipative order is essential if quantitatively accurate predictions for the multiple-time correlation functions is desired.

In principle, in the limit of very small wave vectors, one might expect that the additional couplings in the higher-order correlation arising from the dissipative part of the vertices become less important and may be neglected. In fact, this is not always the case since the overall order in the wave vector of the various terms in the expressions for G^{21} is determined by a wave-vector dependent prefactor (the vertex) multiplied by the time convolution of two-point, two-time correlation functions. The time convolution of functions such as $G_k^{LN}(t)$, which vanish as $k\rightarrow 0$, can give additional factors of the wave vector. Thus, for instance, the contribution from the first term in Eq. (19) (with a vertex of Euler order) is in fact of the same order of magnitude as the contribution from the last two terms, which involve vertices of dissipative order in the hydrodynamic limit.

To obtain smaller wave vectors in a simulation to numerically check these considerations for dense systems in which the mode-coupling effects are important, one would need to simulate larger systems with more particles. There are two difficulties with the simulation method applied to larger systems that make it difficult to obtain good statistics for the higher-order correlation functions. First, since the use of cells is memory intensive and the optimal number of cells scales as the cube of the length of the system, one must utilize a cell structure for the simulations, which is not optimal, leading to a reduction in simulation efficiency. Second, the quality of the statistics for the higher-order correlation functions decreases essentially as the square of the number of particles. It is therefore computationally challenging to obtain accurate simulation results for the higher-order correlation functions for larger systems.

V. SUMMARY AND CONCLUSIONS

In this paper, the predictions for higher-order correlation functions based on the mode-coupling formalism developed in Ref. [15] were evaluated in the hydrodynamic limit for a hard-sphere system at moderate densities and compared to simulation results. It was demonstrated that the mode-coupling theory yields excellent results for all higher-order correlation functions provided that dissipative as well Euler-order vertex coupling terms are included in the theory. The good agreement between the theoretical predictions and the simulation results confirms that the assumptions underlying the mode-coupling theory, of how slow and fast decay of arbitrary densities can be separated in a systematic fashion, are quite reasonable.

In contrast to some mode-coupling theories of simple liquids [18,19], the present mode-coupling theory includes all multilinear densities in the set of slow variables, does not neglect corrections to the ''factorization'' approximation, and

does not assume Gaussian statistical properties of the random noise or fluctuating force. As the formalism allows exact expressions to be obtained for all correlation functions in the thermodynamic limit, it provides a systematic way to examine the various assumptions that must be made in order to predict the time dependence of simple and higher-order correlation functions, or to form comparisons with other theories. Along these lines, it was demonstrated that the ''non-Gaussian'' behavior of the random noise is important for the proper description of the multiple point correlation functions on all time scales. In particular, the Gaussian theory for three-point functions leads to oversimplified coupling vertices that have significant quantitative consequences and more importantly, neglects important couplings to linear densities. Since the mode-coupling theory expresses the multiple-time correlation functions in terms of two-time, higher-order correlation functions, the Gaussian theory has similar deficiencies in describing the three-time correlation function of linear densities.

The calculation of higher-order correlation functions of extensive linear densities in the hydrodynamic regime at low to intermediate densities is computationally intensive. The poor statistics obtained from the simulation arises from averaging quantities of order N^3 to obtain a signal of order N. However, since densities of tagged particles do not scale with the number of particles, higher-order correlation functions of tagged particle densities should not suffer from this problem. The extension of the mode-coupling theory of higher-order correlation functions to nonextensive densities of tagged particles is straightforward, and will be presented in a future publication.

It is obviously desirable to apply the mode-coupling formalism to dense and supercooled liquids where correlation functions exhibit more complicated time behavior. In dense systems, there is compelling evidence [27], which suggests that the eigenmode spectrum of the Liouville operator for simple liquids changes, and a generalized ''heat'' mode becomes long lived even at fairly large wave vectors. At large wave vectors, this mode roughly corresponds to a self-diffusion mode [29] that is slow in dense liquids due to particle caging effects. Within the mode-coupling formalism, the emergence of this short-wavelength collective mode implies that the cutoff wave vector k_c for the heat mode becomes of the order of inverse molecular length scales. Under these circumstances, the mode-coupling correction terms to the expressions for the higher-order correlation functions are not expected to be small and must be considered. Appropriately defined higher-order correlation functions may be quite useful in examining the microscopic origins of complex relaxation behavior and dynamical heterogeneities. To this end, one may examine the higher-order correlation functions at much larger wave vectors using a mode-coupling theory in which the modes forming the basis set for the long-time behavior are associated with physical processes on these length scales. In fact, the structure of the mode-coupling theory suggests that measures of dynamical heterogeneity based on multiple-point correlation functions [10] are quite closely related to measures based on multiple-time correlation functions [11]. These issues are currently being pursued.

APPENDIX: EVALUATION OF THE VERTICES

In this appendix, all vertices used to formulate numerical predictions for higher-order correlation functions are given for the sake of completeness. To leading order in the wave vectors, all vertices are either of Euler order (order k) or of dissipative order (order k^2). Since the second term in the expression for the vertices in Eq. (9) involves two time derivatives of hydrodynamic densities, it is at least of quadratic order in the wave vectors. Therefore the Euler order of any vertex is given by the static correlation function (first term) of Eq. (9). This static correlation function is imaginary and an odd function of the wave vector. The leading order of a vertex of quadratic order in the wave vector is therefore given by the second term in Eq. (9). For the hard-sphere system, all static correlation functions in the zero wave-vector limit can be evaluated exactly if the radial distribution function at contact $g(a) = \chi$ is known. The calculation of the vertices at Euler order is facilitated by considering the identity, valid in the canonical and grand-canonical ensembles,

$$\langle \dot{A}B \rangle = \beta^{-1} \langle \{A,B\} \rangle, \tag{A1}$$

which links the time derivative to a Poisson bracket of the densities. It follows from $\dot{A} = \{A,\mathcal{H}\}$ and from the form of the distribution function,

$$\int \{A,\mathcal{H}\} B e^{-\beta\mathcal{H}} d\Gamma = \int \left[\frac{\partial A}{\partial q} B \frac{\partial \mathcal{H}}{\partial p} - \frac{\partial A}{\partial p} B \frac{\partial \mathcal{H}}{\partial q} \right] e^{-\beta\mathcal{H}} d\Gamma,$$

which, by partial integration, yields

$$\beta^{-1} \int \left[\frac{\partial}{\partial p} \left(B \frac{\partial A}{\partial q} \right) - \frac{\partial}{\partial q} \left(\frac{\partial A}{\partial p} B \right) \right] e^{-\beta\mathcal{H}} d\Gamma$$

$$= \beta^{-1} \int \{A,B\} e^{-\beta\mathcal{H}} d\Gamma.$$

To evaluate the higher-order correlation functions in the text, the vertices $\bar{M}^{TT;L}$ and $\bar{M}^{TL;T}$ are needed. The latter is the simplest, as $Q_2^{TL} = T_{\mathbf{k}-\mathbf{q}} L_{\mathbf{q}}$, so

$$\bar{M}^{TL;T}_{\mathbf{k}-\mathbf{q},\mathbf{q};\mathbf{k}} = \beta^{-1} \langle \{T_{\mathbf{k}-\mathbf{q}} L_q, T_{\mathbf{k}}^*\} \rangle / \langle T_{\mathbf{k}} T_{\mathbf{k}}^* \rangle$$

$$= ik\beta^{-1} \langle T_{\mathbf{k}-\mathbf{q}} T_{\mathbf{k}-\mathbf{q}}^* \rangle / \langle T_{\mathbf{k}} T_{\mathbf{k}}^* \rangle = ik\beta^{-1},$$

where we have used $\{AB,C\} = A\{B,C\} + \{A,C\}B$ and the fact that $\{T_{\mathbf{q}}, T_{\mathbf{k}}^*\} = 0$ and $\{L_{\mathbf{q}}, T_{\mathbf{k}}^*\} = ikT_{\mathbf{k}-\mathbf{q}}^*$.

It is straightforward to show that $Q_2^{TT} = T_{\mathbf{k}-\mathbf{q}} T_{\mathbf{q}} - \frac{2}{3} m E_{\mathbf{k}}$, so using the above result for $\{L, T\}$, we obtain

$$\bar{M}^{TT;L}_{\mathbf{k}-\mathbf{q},\mathbf{q};\mathbf{k}} = -ik\beta^{-1} - \frac{2}{3} \langle \{E_{\mathbf{k}}, L_{\mathbf{k}}^*\} \rangle.$$

The energy can be split into a kinetic and a potential part. The kinetic contribution to $M^{TT;L}$ is easily calculated, and $M^{TT;L}$ can be expressed as

$$\bar{M}^{TT;L}_{\mathbf{k}-\mathbf{q},\mathbf{q};\mathbf{k}}=i\tfrac{2}{3}k\beta^{-1}-\tfrac{2}{3}\langle\{E^{\mathrm{pot}}_{\mathbf{k}},L^{*}_{\mathbf{k}}\}\rangle.$$

The second term on the right-hand side of the equation above can be evaluated by noting that

$$\{E^{\mathrm{pot}}_{\mathbf{k}},L^{*}_{\mathbf{k}}\}=\tfrac{1}{2}\sum_{j\neq m}[e^{i\mathbf{k}\cdot\mathbf{r}_{mj}}-1]\hat{x}\cdot\partial_{\mathbf{r}_{j}}V(r_{mj})$$

$$=-\tfrac{1}{2}\sum_{j\neq m}i(\mathbf{k}\cdot\mathbf{r}_{mj})\hat{x}\cdot\partial_{\mathbf{r}_{m}}V(r_{mj})+O(k^{2}),$$

where $\mathbf{r}_{mj}=\mathbf{r}_{m}-\mathbf{r}_{j}$, which implies

$$\langle\{E^{\mathrm{pot}}_{\mathbf{k}},L^{*}_{\mathbf{k}}\}\rangle=-\tfrac{1}{2}ik\langle N\rangle\rho\int r(\hat{x}\cdot\hat{r})\hat{x}\cdot[\partial_{\mathbf{r}}V(r)]g(r)d\mathbf{r},$$

where $g(r)$ is the radial distribution function. Performing the angular integration and writing $g(r)=h(r)e^{-\beta V(r)}$, so that a partial integration can be performed, leads to

$$\langle\{E^{\mathrm{pot}}_{\mathbf{k}},L^{*}_{\mathbf{k}}\}\rangle=-ik\frac{2\pi\rho\langle N\rangle}{3\beta}\int_{a}^{\infty}\partial_{r}(r^{3}h(\tau))dr=-ikb\rho N\chi,$$

where $b\equiv 2\pi a^{3}/3$ and χ is the radial distribution function at contact. χ can be estimated using the Carnahan-Starling equation of state [20] and the expression for the pressure p of a hard-sphere system,

$$\frac{\beta p}{\rho}=\frac{1+\bar{\eta}+\bar{\eta}^{2}-\bar{\eta}^{3}}{(1-\bar{\eta})^{3}}=1+b\rho\chi,$$

where $\bar{\eta}$ is the packing fraction given by $\bar{\eta}=\pi\rho a^{3}/6$.

Combining all terms, one obtains

$$M^{TT;L}_{\mathbf{k}-\mathbf{q},\mathbf{q};\mathbf{k}}=i\tfrac{2}{3}kp/\rho.$$

Turning now to the calculation of the dissipative part of vertices, their specific wave-vector dependence is determined as follows: The derivative of a conserved density can be written as

$$\dot{A}^{a}_{\mathbf{k}}\approx i\mathbf{k}\cdot J^{a}_{\mathbf{k}},$$

where $J^{a}_{\mathbf{k}}$ is the current associated with the hydrodynamic variable a. What is needed in Eq. (10) is the *dissipative* current $j^{a}_{\mathbf{k}}\equiv(1-\mathcal{P})J^{a}_{\mathbf{k}}$. Looking first at the vertex $\bar{M}^{TH;T}$, using

$$Q^{TH}_{\mathbf{k}-\mathbf{q},\mathbf{q}}=T_{\mathbf{k}-\mathbf{q}}H_{\mathbf{q}}-\frac{\langle T_{\mathbf{k}-\mathbf{q}}H_{\mathbf{q}}T_{-\mathbf{k}}\rangle}{mNk_{B}T}T_{\mathbf{k}}=T_{\mathbf{k}-\mathbf{q}}H_{\mathbf{q}}+\sqrt{\tfrac{2}{3}}T_{\mathbf{k}},$$

the vertex can be expressed as

$$\bar{M}^{TH;T}_{\mathbf{k}-\mathbf{q},\mathbf{q};\mathbf{k}}=-k_{x}(k_{x}-q_{x})v_{h}-k_{x}q_{x}v'_{h}$$

$$-k_{x}^{2}\sqrt{\tfrac{2}{3}}\int_{0}^{\infty}\frac{\langle j^{T}_{\mathbf{k}}(t)j^{T}_{-\mathbf{k}}\rangle}{m\langle N\rangle k_{B}T}dt,\qquad(A2)$$

where

$$v_{h}=\int_{0}^{\infty}\frac{\langle J^{T}_{\mathbf{k}-\mathbf{q}}(t)H_{\mathbf{q}}(t)j^{T}_{-\mathbf{k}}\rangle}{m\langle N\rangle k_{B}T}dt,$$

$$v'_{h}=\int_{0}^{\infty}\frac{\langle T_{\mathbf{k}-\mathbf{q}}(t)J^{H}_{\mathbf{q}}(t)j^{T}_{-\mathbf{k}}\rangle}{m\langle N\rangle k_{B}T}dt.\qquad(A3)$$

Similar expressions can be obtained for the parameters v_{n} and v_{th} appearing in the $M^{TN;T}$ and $M^{TT;H}$ vertices (see Table II). To obtain the leading behavior for small wave vectors, the wave vectors in the integrals can be set to zero, and the projected dynamics Liouvillian in the exponent in Eq. (10) can be replaced by the full Liouvillian. Then, the Green-Kubo expression for the viscosity η can be recognized in the last term of Eq. (A2),

$$\eta=\frac{\beta}{V}\int_{0}^{\infty}\langle j^{T}(t)j^{T}\rangle dt.\qquad(A4)$$

For the viscosity η and the heat conduction λ (which figures in the expression for $\bar{M}^{TT;H}$), we take the Enskog expressions [21],

$$\eta=\eta_{0}b\rho\left(\frac{1}{b\rho\chi}+\frac{4}{5}+0.7614b\rho\chi\right),$$

$$\lambda=\lambda_{0}b\rho\left(\frac{6}{5}+\frac{1}{b\rho\chi}+0.7574b\rho\chi\right).$$

where the Boltzmann value of the shear viscosity η_{0} and thermal diffusivity λ_{0} are given by

$$\eta_{0}=\frac{5}{16a^{2}}\left(\frac{m}{\beta\pi}\right)^{1/2},$$

$$\lambda_{0}=\frac{75}{64a^{2}}k_{B}\left(\frac{m}{\beta\pi}\right)^{1/2}.$$

For the particular parameters of the simulation, it was checked by studying the decay of simple correlation functions that the Enskog expressions are accurate.

In principle, integrals of time correlation functions of products of two currents and a density, as in the expression for v_{h} and v'_{h} in Eq. (A3), can be written in the hydrodynamic limit in terms of transport coefficients and derivatives of transport coefficients with respect to thermodynamic quantities like the temperature and chemical potential. Dissipative contributions such as these have already been evaluated by Lim [30] in the zero wave-vector limit in the context of generalized hydrodynamics. In fact, the expression for v'_{h} can be related to the viscosity [30] as

$$v'_{h}=\left(\frac{2}{3}\right)^{1/2}\frac{\eta}{m\rho},$$

whereas v_h can be expressed in terms of the viscosity and the derivatives of viscosity with respect to the temperature and chemical potential. Using the form for v'_h, $M^{TH;T}_{\mathbf{k}-\mathbf{q},\mathbf{q};\mathbf{k}}$ can be written as

$$\bar{M}^{TH;T}_{\mathbf{k}-\mathbf{q},\mathbf{q};\mathbf{k}} = -k_x(k_x - q_x)\left[v_h - \left(\frac{2}{3}\right)^{1/2}\frac{\eta}{m\rho}\right]. \quad (A5)$$

Since it is not known how well the derivatives with respect

to temperature and energy of the approximate kinetic theory expressions for the transport coefficients correspond to their actual values, v_h, v_n and v_{th} are taken as free parameters that will be fitted from simulation data.

The expressions for the vertices that are needed in the text are listed in Tables I and II. Also tabulated are the vertices one would obtain from a Gaussian theory in which static three-point correlation functions are set to zero. These Gaussian vertices are denoted by V_{21}.

---

[1] R. Böhmer, G. Hinze, G. Diezemann, B. Geil, and H. Sillescu, Europhys. Lett. **36**, 55 (1996).

[2] U. Tracht, M. Wilhelm, A. Heuer, H. Feng, K. Schmidt-Rohr, and H. W. Spiess, Phys. Rev. Lett. **81**, 2727 (1998).

[3] D. A. Blank, L. J. Kaufman, and G. R. Fleming, J. Chem. Phys. **113**, 771 (2000).

[4] V. Astinov, K. J. Kubarych, C. J. Milne, and R. J. D. Miller, Chem. Phys. Lett. **327**, 334 (2000).

[5] O. Golonzka, N. Demirdöven, M. Khalil, and A. Tokmakoff, J. Chem. Phys. **113**, 9893 (2000).

[6] S. Mukamel, A. Piryatinski, and V. Chernyak, Acc. Chem. Res. **32**, 145 (1999).

[7] T. Steffen and K. Duppen, J. Chem. Phys. **106**, 3854 (1997); Phys. Rev. Lett. **76**, 1224 (1996).

[8] T. Keyes and J. T. Fourkas, J. Chem. Phys. **112**, 287 (2000).

[9] W. Kob, C. Donati, S. J. Plimpton, P. H. Poole, and S. C. Glotzer, Phys. Rev. Lett. **79**, 2827 (1997).

[10] S. C. Glotzer, V. N. Novikov, and T. B. Schrøder, J. Chem. Phys. **112**, 509 (2000).

[11] A. Heuer and K. Okun, J. Chem. Phys. **106**, 6176 (1997); A. Heuer, Phys. Rev. E **56**, 730 (1997); B. Doliwa and A. Heuer, Phys. Rev. Lett. **80**, 4915 (1998); B. Doliwa and A. Heuer, J. Phys.: Condens. Matter **11**, A277 (1999).

[12] K. Okumura and Y. Tanimura, J. Chem. Phys. **106**, 1687 (1997).

[13] A. Ma and R. M. Stratt, Ann. Phys. (N.Y.) **85**, 1004 (2000).

[14] R. A. Denny and D. R. Reichman, Phys. Rev. E **63**, 065101(R) (2001).

[15] R. van Zon and J. Schofield, preceding paper, Phys. Rev. E **65**, 011106 (2002).

[16] J. Machta and I. Oppenheim, Physica A **112**, 361 (1982).

[17] J. Schofield, R. Lim, and I. Oppenheim, Physica A **181**, 89 (1992).

[18] K. Kawasaki, Ann. Phys. (Paris) **61**, 1 (1970).

[19] D. Ronis, Physica A **107**, 25 (1981).

[20] N. F. Carnahan and K. E. Starling, J. Chem. Phys. **51**, 635 (1969).

[21] S. Chapman and T. G. Cowling, *The Mathematical Theory of Non-Uniform Gases* (Cambridge University Press, Cambridge, 1970).

[22] B. J. Alder and T. E. Wainwright, J. Chem. Phys. **27**, 1208 (1957).

[23] R. Zwanzig, in *Lectures in Theoretical Physics*, edited by W. E. Britton, B. W. Downs, and J. Downs (Wiley, New York, 1961); R. Zwanzig, Annu. Rev. Phys. Chem. **16**, 667 (1965).

[24] H. Mori, Prog. Theor. Phys. **33**, 423 (1965); **34**, 399 (1965).

[25] B. J. Berne and R. Pecora, *Dynamic Light Scattering* (Wiley, New York, 1976).

[26] D. C. Rapaport, J. Comput. Phys. **34**, 184 (1980).

[27] B. Kamgar-Parsi, E. G. D. Cohen, and I. M. de Schepper, Phys. Rev. A **35**, 4781 (1987).

[28] M. B. Priestly, *Spectral Analysis and Time Series* (Wiley, New York, 1971).

[29] I. M. de Schepper and E. G. D. Cohen, Phys. Rev. A **22**, 287 (1980); J. Stat. Phys. **27**, 223 (1982).

[30] R. Lim, Ph.D. thesis, Massachusetts Institute of Technology, 1985.